$SU(3)_1$ Chiral Spin Liquid on the Square Lattice: A View from Symmetric Projected Entangled Pair States

Ji-Yao Chen,[1,2] Sylvain Capponi,[3] Alexander Wietek,[4] Matthieu Mambrini,[3] Norbert Schuch,[1,2] and Didier Poilblanc[3]

[1]*Max-Planck-Institut für Quantenoptik, Hans-Kopfermann-Straße 1, 85748 Garching, Germany*
[2]*Munich Center for Quantum Science and Technology, Schellingstraße 4, 80799 München, Germany*
[3]*Laboratoire de Physique Théorique, IRSAMC, Université de Toulouse, CNRS, UPS, 31062 Toulouse, France*
[4]*Center for Computational Quantum Physics, Flatiron Institute, 162 5th Avenue, New York 10010, New York, USA*

(Received 21 January 2020; accepted 27 May 2020; published 29 June 2020)

Quantum spin liquids can be faithfully represented and efficiently characterized within the framework of projected entangled pair states (PEPS). Guided by extensive exact diagonalization and density matrix renormalization group calculations, we construct an optimized symmetric PEPS for a $SU(3)_1$ chiral spin liquid on the square lattice. Characteristic features are revealed by the entanglement spectrum (ES) on an infinitely long cylinder. In all three $\mathbb{Z}_3$ sectors, the level counting of the linear dispersing modes is in full agreement with $SU(3)_1$ Wess-Zumino-Witten conformal field theory prediction. Special features in the ES are shown to be in correspondence with bulk anyonic correlations, indicating a fine structure in the holographic bulk-edge correspondence. Possible universal properties of topological $SU(N)_k$ chiral PEPS are discussed.

DOI: 10.1103/PhysRevLett.125.017201

Introduction.—Quantum spin liquids are entangled states of matter in interacting spin systems, supporting fractionalized excitations [1–3]. In two dimension, among the various classes [4], spin liquids with broken time-reversal symmetry, i.e., chiral spin liquids (CSL) [5,6], exhibit chiral topological order [7]. Intimately related to fractional quantum Hall (FQH) states [8], CSL host both anyonic quasiparticles in the bulk [9] and chiral gapless modes on the edge [10]. It was early suggested that, in systems with enhanced $SU(N)$ symmetry, realizable with alkaline-earth atoms loaded in optical lattices [11], CSL can naturally appear [12]. Later on, many $SU(N)_1$ CSL with different N were identified on the triangular lattice [13], while the original proposal on the square lattice [12] remains controversial.

In recent years, projected entangled pair states (PEPS) [14] have emerged as a powerful tool to study quantum spin liquids. In addition to providing competitive variational ground states [15,16], PEPS also offer a powerful framework to encode topological order [17] and construct nonchiral [18,19] and chiral—both Abelian [20,21] and non-Abelian [22]—SU(2) spin liquids. Generically, SU(2) CSL described by PEPS exhibit linearly dispersing chiral branches in the entanglement spectrum (ES) well described by Wess-Zumino-Witten (WZW) $SU(2)_k$ (with $k = 1$ for Abelian CSL) conformal field theory (CFT) for one-dimensional edges [23]. However, to our knowledge, there is no known example of more general $SU(N)$ PEPS with unambiguous chiral edge modes. Thus, it remains unclear whether symmetric PEPS can describe higher $SU(N)$ CSL *faithfully*. In order to address these issues, we propose and investigate a frustrated SU(3) symmetric spin model on the square lattice with a symmetric PEPS ansatz, thereby taking the first step toward describing general $SU(N)_k$ CSL with PEPS.

Model and exact diagonalization.—On every site, we place a three-dimensional spin degree of freedom, transforming as the fundamental representation of SU(3) group. The Hamiltonian, defined on a square lattice, includes the most general SU(3)-symmetric short-range three-site interaction:

$$H = J_1 \sum_{\langle i,j \rangle} P_{ij} + J_2 \sum_{\langle\langle k,l \rangle\rangle} P_{kl} + J_R \sum_{\triangle ijk} (P_{ijk} + P_{ijk}^{-1}) + i J_I \sum_{\triangle ijk} (P_{ijk} - P_{ijk}^{-1}), \quad (1)$$

where the first (second) term corresponds to two-site permutations over all (next-)nearest neighbor bonds, defined as $P_{ij}|\alpha\rangle_i|\beta\rangle_j = |\beta\rangle_i|\alpha\rangle_j$ with $|\alpha\rangle, |\beta\rangle$ the local basis, and the third and fourth terms are three-site (clockwise)

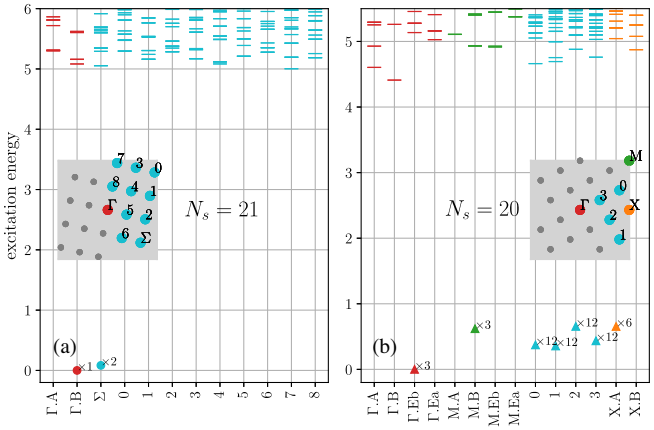

FIG. 1. ED spectra on periodic (a) 21- and (b) 20-site tori. Insets show available momenta in reciprocal space. Dot, triangle, and segment symbols correspond to singlets, $\bar{\mathbf{3}}$, and other finite-dimensional SU(3) irreducible representations (irreps), respectively.

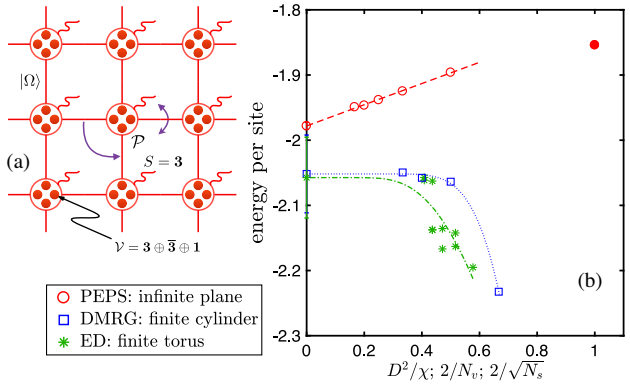

FIG. 2. (a) Symmetric PEPS construction. (b) Comparison of energy densities obtained by symmetric PEPS, DMRG, and ED, plotted versus D^2/χ, $2/N_v$ and $2/\sqrt{N_s}$, respectively. The PEPS energy, optimized at $\chi = D^2$, is further calculated with $\chi = kD^2 (k = 2\text{–}6)$ and extrapolated to $\chi \to \infty$ (red circles). Blue squares stand for DMRG data on finite-width cylinders ($N_v = 3\text{–}6$), keeping up to 4000 states. ED results on tori with $N_s = 12$, 15, 18, 21, 24 sites and different geometries are indicated by stars. Dotted (dash-dotted) line is an exponential fit of the DMRG (ED) data to the thermodynamic limit.

permutations on all triangles of every plaquette. We have chosen $J_2 = J_1/2$ so that the two-body part on the interacting triangular units becomes S_3 symmetric, hence mimicking a triangular lattice [24] and further parametrized the amplitude of each term as $J_1 = 2J_2 = \frac{4}{3}\cos\theta\sin\phi$, $J_R = \cos\theta\cos\phi$, and $J_\mathrm{I} = \sin\theta$.

We have performed extensive exact diagonalization (ED) calculations [25,26] on various periodic N_s-site clusters to locate the CSL phase in parameter space. We expect (1) to host a $\mathrm{SU}(3)_1$ CSL equivalent to the 221 Halperin FQH state [27,28], whose spectral signatures on small tori can be established precisely [29,30]. A careful scan in θ and ϕ reveals a small region where, for $N_s = 3p$ ($p \in \mathbb{N}^+$), there are three low-lying singlets below the octet gap, reflecting the expected topological degeneracy of the CSL. For $N_s \neq 3p$, the low-energy quasidegenerate manifold reflects perfectly the anyon content of the CSL. In both cases, the momenta of low-energy states match the heuristic counting rules of the 221 Halperin state with 0, 1, or 2 quasiholes [30–33]. Also, a 4×4 cluster with open boundaries reveals the expected CFT edge spectrum (see Fig. 1 and Supplemental Material [34]). Hereafter, we focus on angles $\theta = \phi = \pi/4$, for which clear evidence of a gapped CSL is found [35,36].

Symmetric PEPS ansatz.—A symmetric PEPS representation of the CSL enables us to access not only local properties (e.g., energy density) efficiently, but also topological properties from its entanglement structure [37,38]. This can be accomplished by using SU(3)-symmetric tensors, analogously to the SU(2) case [39,40]. The simplest virtual space available here is $\mathcal{V} = \mathbf{3} \oplus \bar{\mathbf{3}} \oplus \mathbf{1}$ (with bond dimension $D = 7$) such that (i) a symmetric maximally entangled SU(3) singlet $|\Omega\rangle$ can be realized on every bond by pairing two neighboring virtual particles and (ii) four virtual particles around each site can be fused into the three-dimensional physical spin with an onsite projector $\mathcal{P}$ [41,42], see Fig. 2(a). In addition to the continuous rotation symmetry, full account of the discrete C_{4v} point-group symmetry (shown as purple arrows in Fig. 2(a)) is taken [40], and tensors are classified according to the corresponding irreps. By linearly combining onsite projectors of two different irreps with opposite ± 1 characters with respect to axis reflections, one can construct a complex PEPS ansatz breaking both parity (P) and time-reversal (T) symmetries while preserving PT [20,22], as required for a CSL ground state (for details, see the Supplemental Material [34]). For later convenience, we define the tensor $\mathcal{A}$ by absorbing adjacent singlets on the right and down bonds around each site into the projector, forming an equivalent way to express the wave function.

The fact that center of the SU(N) group is isomorphic to the $\mathbb{Z}_N$ group allows one to associate a $\mathbb{Z}_3$ charge $Q = +1$ to the physical space of tensor $\mathcal{A}$, while the virtual space carries $\mathbb{Z}_3$ charges $Q = \{+1, -1, 0\}$, i.e., it contains a regular representation of $\mathbb{Z}_3$. Hence, the tensor $\mathcal{A}$ bears an important $\mathbb{Z}_3$ gauge symmetry associated with local charge conservation: $(Z \otimes Z^\dagger \otimes Z \otimes Z^\dagger) \circ \mathcal{A} = \omega\mathcal{A}$, where the action on virtual indices reads as left, right, up, and down, and $\omega = e^{i2\pi/3}$, $Z = \mathrm{diag}(\omega, \omega, \omega, \omega^2, \omega^2, \omega^2, 1)$ is the representation of the $\mathbb{Z}_3$ generator in $\mathcal{V}$. This built-in gauge symmetry is central to topological properties, such as topological degeneracy on the torus and anyonic excitations [17]. Note that the $\mathbb{Z}_3$ gauge symmetry naturally appears from the physical SU(3) and point-group symmetries, and is not a symmetry we imposed *ad hoc*.

Variational optimization.—The best variational ground state is obtained by taking the ansatz $\mathcal{P} = \sum_{a=1}^{N_1} \lambda_1^a \mathcal{B}_1^a + i \sum_{b=1}^{N_2} \lambda_2^b \mathcal{B}_2^b$, where $\mathcal{B}_1^a$ ($\mathcal{B}_2^b$) transforms as B_1 (B_2) irrep of

C_{4v}, N_1 (N_2) is the number of linearly independent projectors in $\mathcal{B}_1$ ($\mathcal{B}_2$) class, and optimizing the (few) variational parameters $\{\lambda_1^a, \lambda_2^b\} \in \mathbb{R}$ with a conjugate-gradient method [43]. For a given tensor, the energy is obtained via the corner transfer matrix renormalization group (CTMRG) method, computing an effective environment of bond dimension χ surrounding an active 2×2 region embedded in the infinite plane (so-called IPEPS) [44–47]. The gradient is then simply obtained by a finite-difference approach [48]. A U(1) quantum number is also used occasionally to speed up the computation [49–51]. The exact contraction scheme corresponds to the limit $\chi \to \infty$.

To establish the relevance of our symmetric PEPS ansatz for the model (1), we compare the PEPS energy density with that obtained by ED on several tori up to size $N_s = 24$ and by the density matrix renormalization group (DMRG) method [52–54] on various finite cylinders, whose details can be found in the Supplemental Material [34]. As shown in Fig. 2(b), the IPEPS energy density turns out to lie close to the finite-size extrapolated values of ED and DMRG data.

Entanglement spectrum.—To get further insight into the nature of the CSL phase, we now explore the properties of our symmetric PEPS, where the $\mathbb{Z}_3$ gauge symmetry implies topological degeneracy on closed manifolds. On finite-width cylinders, quasidegenerate ground states can be constructed by restricting virtual boundaries of PEPS to fixed $\mathbb{Z}_3$ charges $Q = 0, \pm 1$, with or without inserting $\mathbb{Z}_3$ flux line through the cylinder. Here we focus on states without $\mathbb{Z}_3$ flux line and briefly discuss the others in the Supplemental Material [34]. The topological properties can be most easily obtained through a study of the entanglement spectrum, which is defined to be minus log of the spectrum of reduced density matrix (RDM) of subsystem, say the left half of a cylinder [37]. For a PEPS on an infinitely long cylinder, the RDM can be constructed from leading eigenvectors of the transfer operator [38]. Since the onsite tensor carries charge $+1$, the cylinder width N_v must be a multiple of 3. In our setting with bond dimension $D = 7$, exactly contracting the transfer operator is not feasible for moderate N_v. Instead, we use the CTMRG environment tensors to construct approximate leading eigenvectors [21], where large environment dimension χ is needed to achieve convergence [22]. The constructed RDM is fully invariant under translation and SU(3) rotations, which allows one to block diagonalize it, introducing the $\mathbb{Z}_3$ charges (associated with the $\mathbb{Z}_3$ gauge symmetry), two U(1) quantum numbers, and the momentum quantum number. The results with $N_v = 6, \chi = 343$ are shown in Fig. 3 for the three different charge sectors, i.e., $Q = 0, \pm 1$.

Linearly dispersing chiral modes well separated from the high-energy continuum are seen with the same velocity, one mode in the $Q = 0$ sector and three modes in the $Q = +1$ sector. The $Q = \pm 1$ sectors have identical spectra: As both the bare tensor and the bond $|\Omega\rangle$ are PT symmetric, so is the wave function, but after the reflection, the bonds are at the other side of the entanglement cut, and since the bonds exchange $\mathbf{3} \leftrightarrow \bar{\mathbf{3}}$, this maps between the $Q = \pm 1$ spectra. Interestingly, for all different χ we have considered, the lowest level in the $Q = 0$ sector appears at finite momentum $K_0 = -\pi/3$, while the three branches in the $Q = \pm 1$ sectors start at momenta $K_{\pm 1} = -\pi/3, \pi/3$, and π. We believe the momentum shift is due to a quantum of magnetic flux trapped in the cylinder and is an intrinsic property of the optimized PEPS that constrains us to choose $N_v = 6p$, p integer (for $N_v = 3(2p+1)$, where K_0 and $K_{\pm 1}$ do not belong to the reciprocal space, see the Supplemental Material [34]).

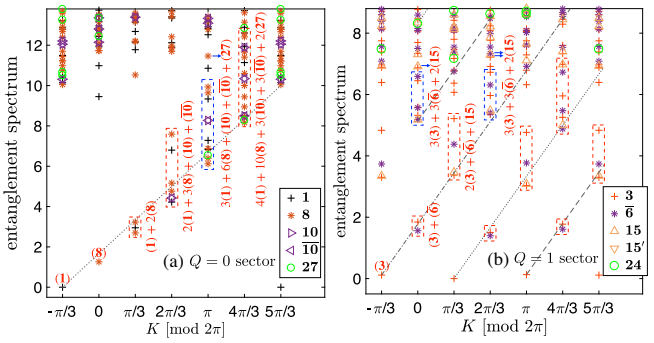

FIG. 3. Entanglement spectrum on an infinitely long $N_v = 6$ cylinder, computed with $\chi = 343$, in the (a) $Q = 0$ and (b) $Q = +1$ sectors. The spectrum in the $Q = -1$ sector, found to be identical to that in the $Q = +1$ sector but with conjugated SU(3) irreps, is shown in the Supplemental Material [34]. For convenience, the lowest eigenvalue is subtracted in each plot. One chiral branch is seen in (a) starting at momentum $K_0 = -\pi/3$ and three branches are identified in (b) starting at momenta $K_{\pm 1} = -\pi/3, \pi/3$, and π. In each sector, the irreps encircled by red boxes (or blue boxes and arrows) agree with the level counting of the $\mathrm{SU}(3)_1$ WZW CFT (shown on the plot vertically).

Reconstructing the SU(3) irreps from the two U(1) quantum numbers (corresponding Young tableaux are provided in the Supplemental Material [34]), we found that the level contents follow the prediction of the Virasoro levels of the $\mathrm{SU}(3)_1$ WZW CFT [23,55]. However, we observe a tripling of the branches in the $Q = \pm 1$ sectors, which we shall discuss later.

Bulk correlations.—The above entanglement spectrum provides strong evidence of $\mathrm{SU}(3)_1$ chiral topological order. However, it has been shown that, in PEPS describing chiral phases, certain bulk correlation lengths computed from the transfer matrix spectrum diverge [20–22,56–61]. Nevertheless, *a priori* it is not known which type of correlation is quasi-long-ranged and how critical bulk correlations are related to the observed chiral edge modes. Here we address this question with our symmetric PEPS ansatz.

Within the PEPS methodology, correlation lengths of different types of operators, including the anyonic type, can be obtained from two complementary methods. On one hand, correlation functions of usual local operators, e.g., spin-spin correlation $C_s(d) = \langle \mathbf{S}_i \cdot \mathbf{S}_{i+d\mathbf{e}_x} \rangle$ or dimer-dimer correlation $C_d(d) = \langle D_i^x D_{i+d\mathbf{e}_x}^x \rangle - \langle D_i^x \rangle \langle D_{i+d\mathbf{e}_x}^x \rangle$, can be obtained by applying local operators on the physical indices. Here the spin operators are the eight generators of the su(3) algebra, and the dimer operator is $D_i^x = \mathbf{S}_i \cdot \mathbf{S}_{i+\mathbf{e}_x}$. The $\mathbb{Z}_3$ gauge symmetry enables us to define topologically nontrivial local excitations like spinon, vison, and their bound state [17,39,62]. A spinon excitation can be created by applying an operator X satisfying $XZ = \omega ZX$ on the virtual index of local tensor such that it carries zero $\mathbb{Z}_3$ charge instead of the original charge 1. Similarly, X^2 can create a charge -1 spinon, since $X^2 Z = \omega^2 Z X^2$. A pair of vison excitations can be created by putting a string of Z (or Z^2) operators on the virtual level, whose end points correspond to the visons. Parafermions, bound states of a spinon and a vison [41,62], can be created by putting spinons at the end points of the Z string. All these real space correlations obtained using the CTMRG environment tensors (see the Supplemental Material [34] for further details) are shown in Fig. 4(a).

On the other hand, correlation lengths can also be extracted from the spectrum of transfer matrix, constructed with CTMRG environment tensors (see the Supplemental Material [34]), whose eigenvalue degeneracies carry information about the types of correlation. Correlation lengths along horizontal and vertical directions are found to be the same, as expected. Denoting the distinct transfer matrix eigenvalues as t_a $(a = 0, 1, \ldots)$ with $|t_0| > |t_1| > |t_2| > \cdots$, it turns out t_0 is nondegenerate, suggesting absence of long-range order in the variational wave function (confirming ED results). The subleading eigenvalues t_a $(a = 1, 2, 3)$ are sixfold degenerate, followed by a nondegenerate t_4. These eigenvalues give direct access to series of correlation lengths $\xi^{(a)} = -1/\log(|t_a/t_0|)$, which therefore carry the same degeneracies. We have also computed the correlation length with a ± 1 $\mathbb{Z}_3$ flux by inserting a string of Z (or Z^2) operators, where the leading eigenvalue of the corresponding transfer matrix is denoted as $t_{Z,1}$ [63]. From $t_{Z,1}$, which is nondegenerate, one obtains the leading correlation length in the flux sector $\xi_Z^{(1)} = -1/\log(|t_{Z,1}/t_0|)$.

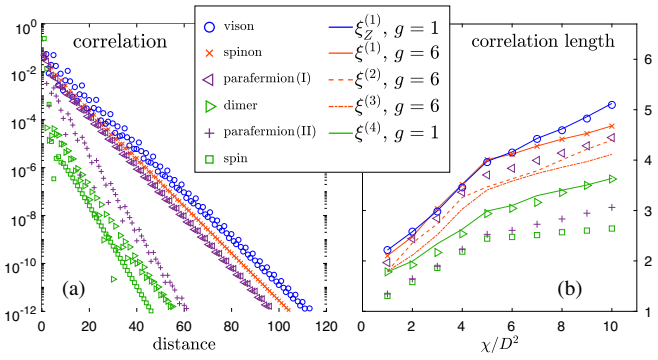

FIG. 4. Different bulk correlations in the optimized PEPS. From the correlations versus distance (computed with $\chi = 392$) in (a), we extract the correlation lengths using exponential fits, which are shown in (b) (using the same symbols), along with those extracted from the transfer matrix spectrum with or without flux inserted (shown as lines), with g the degeneracy of the eigenvalue. Both approaches agree for the spinon, vison, and dimer correlation lengths, which show no saturation with increasing χ.

A summary of various correlation lengths versus χ from both methods is shown in Fig. 4(b). We find that the largest one in all sectors, $\xi_Z^{(1)}$, is equal to the correlation length found between a pair of visons; it is nondegenerate, in agreement with the fact that visons carry no spin. In the sector without flux, the leading correlation length $\xi^{(1)}$ perfectly agrees with the one extracted from placing a spinon-antispinon pair. Moreover, since PT symmetry maps spinons placed on reflected bonds to antispinons, we expect the spinon correlations to have a degeneracy structure $\mathbf{3} \oplus \bar{\mathbf{3}}$, which is indeed consistent with the sixfold degeneracy in $\xi^{(1)}$ and further supported by checking the U(1) quantum numbers of the t_1 multiplet. The U(1) quantum numbers further suggest that $t_{2,3}$, which are also sixfold degenerate, also carry SU(3) representation $\mathbf{3} \oplus \bar{\mathbf{3}}$. Thus, $\xi^{(1,2,3)}$ all correspond to spinon correlation lengths. This, in fact, is in correspondence with the three linearly dispersing branches in the ES in the $Q = \pm 1$ charged sectors, as we shall discuss later. Examining further, we find $\xi^{(4)}$ is identical to dimer correlation length, where nondegeneracy agrees with dimer operator being SU(3) rotation invariant. Depending on the parafermion type, the $\xi_{\text{parafermion}}$ have different values, both of which are smaller than the spinon correlation length. Interestingly, all these correlation lengths, except the spin correlation length, have no sign of saturation with increasing χ, in agreement with our expectation that the state is *not* in the $\mathbb{Z}_3$ quantum double phase.

Degeneracy structure of topological chiral PEPS.—A remarkable feature of our results is the correspondence between the leading four eigenvalues of the transfer matrix and the different sectors in the ES: The $Q = 0$ sector has one branch, while $Q = \pm 1$ each have three almost degenerate branches. This is in direct analogy to the unique leading eigenvalue t_0, which has trivial spin, and the approximate threefold degeneracy of t_1, t_2, and t_3, which have perfectly degenerate spins $\mathbf{3}$ and $\bar{\mathbf{3}}$, matching the perfect degeneracy between $Q = \pm 1$. A similar correspondence between (approximate) degeneracy of the (2D) transfer operator and of the ES branches was observed for chiral PEPSs with $\mathrm{SU}(2)_1$ counting, where it could be explained as arising from the symmetry of the tensors, and subsequently used to remove the degeneracy in the

nontrivial sector in the vicinity of a (fine-tuned) perfectly degenerate point [61]. Furthermore, we checked that the same correspondence also holds in the PEPS description of non-Abelian $SU(2)_2$ CSL [22]. It is suggestive that such a correspondence in the (approximate) degeneracy structure is a general feature of chiral PEPS and will also hold for general $SU(N)_k$ models; indeed, both ES and the eigenvalues t_i are extracted from the same objects, namely, the fixed points of the CTMRG environment. It would be interesting to see whether such a correspondence could help resolve the additional chiral branches in ES of general chiral models and further characterize the precise nature of a chiral theory.

Conclusion and outlook.—In this Letter, we have proposed a model for a $SU(3)_1$ CSL on the square lattice and, by ED techniques, unambiguously identified the relevant parameter space. We have then focused on constructing and optimizing a *symmetric* PEPS ansatz for the CSL, whose variational energy is remarkably good as compared to ED and DMRG data. For the first time, linear dispersing branches in all three sectors of $SU(3)_1$ WZW CFT can be obtained with PEPS. A comparison between edge spectrum and bulk correlations reveal a fine structure in the bulk-edge correspondence, which will be tested in further study of $SU(N)_k$ PEPS CSL. Certain unresolved issues, e.g., anyon statistics of chiral topological order, remain open, which we hope to uncover in the future.

We acknowledge useful conversations with M. Arildsen, C. Delcamp, A. Hackenbroich, M. Iqbal, A. Ludwig, G. Sierra, and J. Slingerland. J. Y. C. and N. S. acknowledge support by the European Union's Horizon 2020 Programme through the ERC Starting Grant WASCOSYS (Grant No. 636201) and from the DFG (German Research Foundation) under Germany's Excellence Strategy (EXC-2111–390814868). D. P. acknowledges support by the TNSTRONG ANR-16-CE30-0025 and TNTOP ANR-18-CE30-0026-01 grants awarded by the French Research Council. The authors were granted access to the HPC resources of CALMIP and GENCI supercomputing centers under the allocation 2017-P1231 and A0030500225, respectively, and computations were also carried out on the TQO cluster of the Max-Planck-Institute of Quantum Optics.

[1] G. Misguich and C. Lhuillier, Two-dimensional quantum antiferromagnets, in *Frustrated Spin Systems*, edited by H. T. Diep (World Scientific, Singapore, 2005), pp. 229–306.
[2] L. Savary and L. Balents, Quantum spin liquids: A review, Rep. Prog. Phys. **80**, 016502 (2017).
[3] Y. Zhou, K. Kanoda, and T.-K. Ng, Quantum spin liquid states, Rev. Mod. Phys. **89**, 025003 (2017).
[4] X.-G. Wen, Quantum orders and symmetric spin liquids, Phys. Rev. B **65**, 165113 (2002).
[5] V. Kalmeyer and R. B. Laughlin, Equivalence of the Resonating-Valence-Bond and Fractional Quantum Hall States, Phys. Rev. Lett. **59**, 2095 (1987).
[6] X. G. Wen, F. Wilczek, and A. Zee, Chiral spin states and superconductivity, Phys. Rev. B **39**, 11413 (1989).
[7] X. G. Wen, Topological orders in rigid states, Int. J. Mod. Phys. B **04**, 239 (1990).
[8] D. C. Tsui, H. L. Stormer, and A. C. Gossard, Two-Dimensional Magnetotransport in the Extreme Quantum Limit, Phys. Rev. Lett. **48**, 1559 (1982).
[9] B. I. Halperin, Statistics of Quasiparticles and the Hierarchy of Fractional Quantized Hall States, Phys. Rev. Lett. **52**, 1583 (1984).
[10] X. G. Wen, Gapless boundary excitations in the quantum Hall states and in the chiral spin states, Phys. Rev. B **43**, 11025 (1991).
[11] A. V. Gorshkov, M. Hermele, V. Gurarie, C. Xu, P. S. Julienne, J. Ye, P. Zoller, E. Demler, M. D. Lukin, and A. M. Rey, Two-orbital SU(N) magnetism with ultracold alkaline-earth atoms, Nat. Phys. **6**, 289 (2010).
[12] M. Hermele, V. Gurarie, and A. M. Rey, Mott Insulators of Ultracold Fermionic Alkaline Earth Atoms: Underconstrained Magnetism and Chiral Spin Liquid, Phys. Rev. Lett. **103**, 135301 (2009).
[13] P. Nataf, M. Lajkó, A. Wietek, K. Penc, F. Mila, and A. M. Läuchli, Chiral Spin Liquids in Triangular-Lattice SU(N) Fermionic Mott Insulators with Artificial Gauge Fields, Phys. Rev. Lett. **117**, 167202 (2016).
[14] F. Verstraete and J. I. Cirac, Renormalization algorithms for quantum-many body systems in two and higher dimensions, arXiv:condmat/0407066.
[15] H. J. Liao, Z. Y. Xie, J. Chen, Z. Y. Liu, H. D. Xie, R. Z. Huang, B. Normand, and T. Xiang, Gapless Spin-Liquid Ground State in the $s = 1/2$ Kagome Antiferromagnet, Phys. Rev. Lett. **118**, 137202 (2017).
[16] H.-Y. Lee, R. Kaneko, T. Okubo, and N. Kawashima, Gapless Kitaev Spin Liquid to Classical String Gas through Tensor Networks, Phys. Rev. Lett. **123**, 087203 (2019).
[17] N. Schuch, J. I. Cirac, and D. Pérez-García, PEPS as ground states: Degeneracy and topology, Ann. Phys. (Amsterdam) **325**, 2153 (2010).
[18] N. Schuch, D. Poilblanc, J. I. Cirac, and D. Pérez-García, Resonating valence bond states in the PEPS formalism, Phys. Rev. B **86**, 115108 (2012).
[19] J.-Y. Chen and D. Poilblanc, Topological $\mathbb{Z}_2$ resonating-valence-bond spin liquid on the square lattice, Phys. Rev. B **97**, 161107(R) (2018).
[20] D. Poilblanc, J. I. Cirac, and N. Schuch, Chiral topological spin liquids with projected entangled pair states, Phys. Rev. B **91**, 224431 (2015).
[21] D. Poilblanc, N. Schuch, and I. Affleck, $SU(2)_1$ chiral edge modes of a critical spin liquid, Phys. Rev. B **93**, 174414 (2016).
[22] J.-Y. Chen, L. Vanderstraeten, S. Capponi, and D. Poilblanc, Non-Abelian chiral spin liquid in a quantum antiferromagnet revealed by an iPEPS study, Phys. Rev. B **98**, 184409 (2018).
[23] P. Francesco, P. Mathieu, and D. Sénéchal, *Conformal Field Theory* (Springer-Verlag, New York, 1997).

[24] The CSL phase should also exist away from $J_2 = J_1/2$, due to its gapped nature.
[25] N. Laflorencie and D. Poilblanc, Simulations of pure and doped low-dimensional spin-1/2 gapped systems, in *Quantum Magnetism*, edited by U. Schollwöck, J. Richter, D. J. J. Farnell, and R. F. Bishop (Springer Berlin, Berlin, 2004), pp. 227–252.
[26] A. W. Sandvik, Computational studies of quantum spin systems, AIP Conf. Proc. **1297**, 135 (2010).
[27] B. I. Halperin, Theory of the quantized Hall conductance, Helv. Phys. Acta **56**, 75 (1983), https://www.e-periodica.ch/digbib/view?pid=hpa-001:1983:56::1243#87.
[28] E. Ardonne and K. Schoutens, New Class of Non-Abelian Spin-Singlet Quantum Hall States, Phys. Rev. Lett. **82**, 5096 (1999).
[29] Y.-H. Wu and H.-H. Tu, Possible su(3) chiral spin liquid on the Kagome lattice, Phys. Rev. B **94**, 201113(R) (2016).
[30] A. Sterdyniak, C. Repellin, B. A. Bernevig, and N. Regnault, Series of Abelian and non-Abelian states in $c > 1$ fractional Chern insulators, Phys. Rev. B **87**, 205137 (2013).
[31] N. Regnault and B. A. Bernevig, Fractional Chern Insulator, Phys. Rev. X **1**, 021014 (2011).
[32] B. A. Bernevig and N. Regnault, Emergent many-body translational symmetries of Abelian and non-Abelian fractionally filled topological insulators, Phys. Rev. B **85**, 075128 (2012).
[33] B. Estienne and B. A. Bernevig, Spin-singlet quantum Hall states and jack polynomials with a prescribed symmetry, Nucl. Phys. **B857**, 185 (2012).
[34] See Supplemental Material at http://link.aps.org/supplemental/10.1103/PhysRevLett.125.017201, in which we provide relevant details of this Letter, including basic knowledge of SU(3) group [64] and permutation operators, ED study on various small clusters, DMRG study on finite cylinders, construction and optimization of SU(3) symmetric PEPS, additional data for ES, and topological excitation and correlation function of symmetric PEPS. In the end, we also list the nonzero elements of the tensors.
[35] Since our model possesses one SU(3) fermion per unit cell, the Lieb-Schultz-Mattis theorem for SU(N) spin systems and its generalization to two dimensions [65–68] imply that a uniform gapped phase is topological.
[36] Long-range parent Hamiltonian for $SU(3)_1$ CSL has been proposed in Refs. [69,70].
[37] H. Li and F. D. M. Haldane, Entanglement Spectrum as a Generalization of Entanglement Entropy: Identification of Topological Order in Non-Abelian Fractional Quantum Hall Effect States, Phys. Rev. Lett. **101**, 010504 (2008).
[38] J. I. Cirac, D. Poilblanc, N. Schuch, and F. Verstraete, Entanglement spectrum and boundary theories with projected entangled-pair states, Phys. Rev. B **83**, 245134 (2011).
[39] S. Jiang and Y. Ran, Symmetric tensor networks and practical simulation algorithms to sharply identify classes of quantum phases distinguishable by short-range physics, Phys. Rev. B **92**, 104414 (2015).
[40] M. Mambrini, R. Orús, and D. Poilblanc, Systematic construction of spin liquids on the square lattice from tensor networks with SU(2) symmetry, Phys. Rev. B **94**, 205124 (2016).
[41] I. Kurečić, L. Vanderstraeten, and N. Schuch, Gapped su(3) spin liquid with $\mathbb{Z}_3$ topological order, Phys. Rev. B **99**, 045116 (2019).
[42] X.-Y. Dong, J.-Y. Chen, and H.-H. Tu, Su(3) trimer resonating-valence-bond state on the square lattice, Phys. Rev. B **98**, 205117 (2018).
[43] J. Nocedal and S. J. Wright, *Numerical Optimization*, 2nd ed. (Springer, New York, 2006).
[44] T. Nishino and K. Okunishi, Corner transfer matrix renormalization group method, J. Phys. Soc. Jpn. **65**, 891 (1996).
[45] R. Orús and G. Vidal, Simulation of two-dimensional quantum systems on an infinite lattice revisited: Corner transfer matrix for tensor contraction, Phys. Rev. B **80**, 094403 (2009).
[46] P. Corboz, T. M. Rice, and M. Troyer, Competing States in the $t - J$ Model: Uniform d-Wave State Versus Stripe State, Phys. Rev. Lett. **113**, 046402 (2014).
[47] M. T. Fishman, L. Vanderstraeten, V. Zauner-Stauber, J. Haegeman, and F. Verstraete, Faster methods for contracting infinite two-dimensional tensor networks, Phys. Rev. B **98**, 235148 (2018).
[48] D. Poilblanc and M. Mambrini, Quantum critical phase with infinite projected entangled paired states, Phys. Rev. B **96**, 014414 (2017).
[49] B. Bauer, P. Corboz, R. Orús, and M. Troyer, Implementing global Abelian symmetries in projected entangled-pair state algorithms, Phys. Rev. B **83**, 125106 (2011).
[50] S. Singh, R. N. C. Pfeifer, and G. Vidal, Tensor network states and algorithms in the presence of a global U(1) symmetry, Phys. Rev. B **83**, 115125 (2011).
[51] A. Weichselbaum, Non-Abelian symmetries in tensor networks: A quantum symmetry space approach, Ann. Phys. (Amsterdam) **327**, 2972 (2012).
[52] S. R. White, Density Matrix Formulation for Quantum Renormalization Groups, Phys. Rev. Lett. **69**, 2863 (1992).
[53] We have used the ITensor C++ library, available at http://itensor.org for our calculations.
[54] E. M. Stoudenmire and S. R. White, Studying two-dimensional systems with the density matrix renormalization group, Annu. Rev. Condens. Matter Phys. **3**, 111 (2012).
[55] P. Bouwknegt and K. Schoutens, The $SU(n)_1$ WZW models: Spinon decomposition and Yangian structure, Nucl. Phys. **B482**, 345 (1996).
[56] T. B. Wahl, H.-H. Tu, N. Schuch, and J. I. Cirac, Projected Entangled-Pair States can Describe Chiral Topological States, Phys. Rev. Lett. **111**, 236805 (2013).
[57] J. Dubail and N. Read, Tensor network trial states for chiral topological phases in two dimensions and a no-go theorem in any dimension, Phys. Rev. B **92**, 205307 (2015).
[58] S. Yang, T. B. Wahl, H.-H. Tu, N. Schuch, and J. I. Cirac, Chiral Projected Entangled-Pair State with Topological Order, Phys. Rev. Lett. **114**, 106803 (2015).
[59] N. Read, Compactly-supported Wannier functions and algebraic k-theory, Phys. Rev. B **95**, 115309 (2017).
[60] D. Poilblanc, Investigation of the chiral antiferromagnetic Heisenberg model using projected entangled pair states, Phys. Rev. B **96**, 121118(R) (2017).
[61] A. Hackenbroich, A. Sterdyniak, and N. Schuch, Interplay of su(2), point group, and translational symmetry for

projected entangled pair states: Application to a chiral spin liquid, Phys. Rev. B **98**, 085151 (2018).

[62] K. Duivenvoorden, M. Iqbal, J. Haegeman, F. Verstraete, and N. Schuch, Entanglement phases as holographic duals of anyon condensates, Phys. Rev. B **95**, 235119 (2017).

[63] Spectrum of transfer matrices inserted with one Z or Z^2 string have the same absolute values but with different phase ω or ω^2.

[64] A. O. Barut and R. Raczka, The explicit construction of finite-dimensional irreducible representations, in *Theory of Group Representations and Applications* (PWN—Polish Scientific Publishers, Warszawa, 1980), pp. 277–316.

[65] E. Lieb, T. Schultz, and D. Mattis, Two soluble models of an antiferromagnetic chain, Ann. Phys. (N.Y.) **16**, 407 (1961).

[66] M. Oshikawa, Commensurability, Excitation Gap, and Topology in Quantum Many-Particle Systems on a Periodic Lattice, Phys. Rev. Lett. **84**, 1535 (2000).

[67] M. B. Hastings, Sufficient conditions for topological order in insulators, Europhys. Lett. **70**, 824 (2005).

[68] K. Totsuka, Lieb-Schultz-Mattis approach to SU(N)-symmetric Mott insulators, JPS 72nd Annual Meeting (2017).

[69] H.-H. Tu, A. E. B. Nielsen, and G. Sierra, Quantum spin models for the $\mathrm{SU}(n)_1$ Wess-Zumino-Witten model, Nucl. Phys. **B886**, 328 (2014).

[70] R. Bondesan and T. Quella, Infinite matrix product states for long-range su(n) spin models, Nucl. Phys. **B886**, 483 (2014).